• Basic Research •

Catalpol ameliorates diabetic retinal vascular endothelial injury by suppressing NLRP3 inflammasome *via* targeting METTL3-m^{6}A modification

Jing-Yu Liu[1,2], Jun-Ya Zhu[1,3], Yi-Fang Xiao[4], Yi-Rui Ge[2], Feng Yan[5], Qin Jiang[1,3]

[1]The Fourth Clinical Medical College, Nanjing Medical University, Nanjing 211166, Jiangsu Province, China
[2]Department of Ophthalmology, Jinling Hospital Affiliated to Nanjing University, Nanjing 210000, Jiangsu Province, China
[3]The Affiliated Eye Hospital, Nanjing Medical University, Nanjing 210029, Jiangsu Province, China
[4]School of Pharmacy, China Pharmaceutical University, Nanjing 211198, Jiangsu Province, China
[5]Department of Ophthalmology, Taikang Xianlin Gulou Hospital, Nanjing 210023, Jiangsu Province, China
Correspondence to: Qin Jiang. The Fourth Clinical Medical College of Nanjing Medical University; The Affiliated Eye Hospital, Nanjing Medical University, Nanjing 210029, Jiangsu Province, China. jqin710@vip.sina.com; Feng Yan. Department of Ophthalmology, Taikang Xianlin Gulou Hospital, Nanjing 210023, Jiangsu Province, China. yanfengdoctor@126.com
Received: 2025-12-21 Accepted: 2026-02-25

Abstract

● **AIM:** To investigate whether catalpol protects against diabetic retinal vascular endothelial injury by targeting the methyltransferase-like 3 (METTL3)-m^{6}A-thioredoxin-interacting protein (TXNIP) axis and inhibiting nucleotide-binding oligomerization domain (NOD)-like receptor family pyrin domain containing 3 (NLRP3) inflammasome activation.

● **METHODS:** A streptozotocin-induced diabetic mouse model (n=20 per group) was used to assess retinal function *via* electroretinogram (ERG) and vascular integrity *via* Evans Blue leakage. Human retinal vascular endothelial cells (HRVECs) were exposed to high glucose (HG, 30 mmol/L) with or without catalpol or the METTL3 inhibitor STM2457. NLRP3 inflammasome components (Western blot), oxidative stress (DCFH-DA probe), global m^{6}A levels (Dot blot), and TXNIP expression were measured. The binding of catalpol to METTL3, NLRP3, TXNIP, and interleukin-1β (IL-1β) was analyzed *via* molecular docking and dynamics simulations.

● **RESULTS:** Catalpol treatment improved ERG amplitudes [a-wave, b-wave, oscillatory potentials (OPs)] and reduced vascular leakage in diabetic mice (P<0.05), while downregulating retinal vascular endothelial growth factor (VEGF), NLRP3, IL-1β, and IL-18 protein levels. In HG-stimulated HRVECs, catalpol inhibited the NLRP3-apoptosis-associated speck-like protein containing a CARD (ASC)-caspase-1 inflammasome, reduced reactive oxygen species, and suppressed METTL3 expression and global m^{6}A methylation (P<0.05). It also attenuated HG-induced TXNIP upregulation. METTL3 inhibition by STM2457 mimicked all protective effects of catalpol. Molecular simulations confirmed stable binding of catalpol to METTL3, NLRP3, TXNIP, and IL-1β.

● **CONCLUSION:** Catalpol alleviates diabetic retinal vascular endothelial injury by inhibiting the NLRP3 inflammasome. This effect is mediated, at least in part, through downregulating METTL3-dependent m^{6}A RNA methylation of TXNIP.

● **KEYWORDS:** catalpol; diabetic retinopathy; NLRP3 inflammasome; METTL3; m^{6}A methylation

DOI:10.18240/ijo.2026.06.03

Citation: Liu JY, Zhu JY, Xiao YF, Ge YR, Yan F, Jiang Q. Catalpol ameliorates diabetic retinal vascular endothelial injury by suppressing NLRP3 inflammasome *via* targeting METTL3-m^{6}A modification. *Int J Ophthalmol* 2026;19(6):1038-1047

INTRODUCTION

Diabetic retinopathy (DR), a leading cause of blindness worldwide, is fundamentally a neurovascular disease driven by chronic low-grade inflammation and retinal endothelial dysfunction[1-2]. Among various inflammatory pathways, the nucleotide-binding oligomerization domain (NOD)-like receptor family pyrin domain containing 3 (NLRP3) inflammasome has emerged as a crucial mediator. Its activation leads to caspase-1-dependent maturation and release of pro-inflammatory cytokines such as interleukin-1β (IL-1β) and IL-18, exacerbating vascular damage and blood-retinal barrier breakdown in DR[3-5].

Catalpol, an iridoid glycoside derived from the traditional Chinese medicine *Rehmannia glutinosa*, has demonstrated broad anti-diabetic, anti-inflammatory, and antioxidant properties in various complication models[6-8]. However, its specific effects and mechanisms on diabetic retinal microvasculature remain largely unexplored.

Recent advances highlight the role of epitranscriptomic regulation, particularly N6-methyladenosine (m^6A) RNA modification, in fine-tuning inflammatory responses[9]. The methyltransferase-like 3 (METTL3), as the core catalytic component, governs m^6A deposition. Importantly, METTL3-dependent m^6A modification has been implicated in stabilizing pro-inflammatory transcripts, including thioredoxin-interacting protein (TXNIP), a key molecular bridge linking oxidative stress to NLRP3 inflammasome activation[10-11]. While METTL3 is upregulated in diabetic vascular complications[12], its function in DR pathogenesis, and whether it can be pharmacologically targeted, is unknown.

We hypothesized that catalpol protects against diabetic retinal endothelial injury by attenuating NLRP3 inflammasome activation, and that this effect is mediated through the inhibition of the METTL3-m^6A-TXNIP axis. This study integrates *in vivo* diabetic models, *in vitro* endothelial cell assays, and computational simulations to test this hypothesis, aiming to reveal a novel epitranscriptomic mechanism for catalpol and identify a potential therapeutic strategy for DR.

MATERIALS AND METHODS

Ethical Approval All procedures were conducted in accordance with the guidelines of the Association for Research in Vision and Ophthalmology (ARVO) and approved by the Animal Ethics Committee of Nanjing Medical University (Ethical Review Approval Number: 2021DZDWLS-001).

Overview of Research Design This study combines *in vivo* animal experiments, *in vitro* cell models, and computer simulations to explore the protective effect of catalpol on DR and its underlying molecular mechanism. The animal experiments evaluate the influence of catalpol on retinal function and vascular integrity in diabetic mice. The cell experiments utilize a high-glucose-induced human retinal vascular endothelial cells (HRVECs) injury model to examine the regulatory effect of catalpol on the NLRP3 inflammasome and m^6A methylation modification. Computational simulations are employed to analyze the binding characteristics of catalpol with key targets.

In vivo Experiments

Animals and establishment of diabetic models Male C57BL/6J mice (8 weeks old, weighing approximately 20 g) were purchased from the Animal Experiment Center of Nanjing Medical University.

Eighty mice were randomly divided into four groups (n=20/group): normal control group (WT), diabetic model group (DM), catalpol treatment group (DM+CAT), and catalpol solvent control group (WT+CAT). Diabetes was induced by a single intraperitoneal injection of streptozotocin (STZ; dissolved in sodium citrate buffer, pH 4.5; Biosharp Company, USA). Three days after injection, a continuous blood glucose level above 16.7 mmol/L in the tail vein for more than 1wk was considered a successful model establishment.

Administration regimen and sample collection After successful modeling, the catalpol treatment group was given catalpol (Beyotime Biotechnology, China) solution at a dose of 5 mg/kg by gavage, 5 times a week for 14wk; the control group was given an equal volume of solvent. Body weight, random blood glucose, and water intake were monitored weekly. At the end of the intervention, electroretinogram (ERG) and vascular leakage detection were performed. Subsequently, the mice were sacrificed and the eyeballs were removed for subsequent protein and RNA analysis.

Retinal function and vascular leakage detection ERG: After 8h of dark adaptation, mice were anesthetized and dilated under red light. Dark-adapted maximal responses (rod-cone response) and oscillatory potentials (OPs) were recorded using corneal ring electrodes (visual electrophysiological instrument, Roland Company, Germany). Evans blue (EB) vascular leakage assay: EB dye (30 g/L; Biosharp Company, USA) was injected through the femoral vein. After 40min, the eyeballs were removed and fixed, and the retinas were separated and spread on a glass slide. The fluorescence intensity of EB was observed and quantitatively analyzed under a fluorescence microscope (Carl Zeiss, Germany) to evaluate the permeability of the blood-retinal barrier[13].

In vitro Experiments

Cell culture and treatment HRVECs were purchased from Cell Systems, USA, and cultured in Dulbecco's modified eagle medium (DMEM) medium (ScienCell Company, USA) supplemented with 10% fetal bovine serum (FBS; Gibco Company, USA).

To establish a high glucose (HG) injury model, cells were divided into a normal glucose group (NG; 5.5 mmol/L D-glucose; Sigma, USA) and a HG group (30 mmol/L D-glucose), and treated for 48h. Catalpol or METTL3 inhibitor STM2457 was added 1h before HG stimulation.

Cell viability and apoptosis detection MTT assay (Biosharp Company, USA) was used to detect cell viability and determine the safe working concentration of catalpol (0.5 mmol/L). Calcein-acetoxymethyl ester (AM)/propidium iodide (PI; Beyotime Biotechnology, China) double staining was used to distinguish live cells (green fluorescence) from dead cells (red fluorescence), and observe cell morphology and membrane integrity. TUNEL staining (Beyotime Biotechnology,

Table 1 Sequences of primers used for RT-qPCR

Gene name	Gene symbol	Forward primer (5′-3′)	Reverse primer (5′-3′)
N6-methyladenosine methyltransferase-like 3	*METTL3*	ACGGAGTCTCGCTCTGTCACC	AGGAGGCTAAGGCAGGAGAATGG
Thioredoxin-interacting protein	*TXNIP*	GGTCTTTAACGACCCTGAAAAGG	ACACGAGTAACTTCACACACCT
Caspase-1	*CASP-1*	TTTCCGCAAGGTTCGATTTTCA	GGCATCTGCGCTCTACCATC
Apoptosis-associated speck-like protein containing a CARD	*PYCARD*	TGGATGCTCTGTACGGGAAG	CCAGGCTGGTGTGAAACTGAA
Interleukin-1 beta	*IL1β*	TGATGTGCTCACTGCCTGGTTTC	GTTGATGTGCTGCGCGAGATTTG
NLR family pyrin domain containing 3	*NLRP3*	TTTCCCTCACCCGACCATTCTC	TTAAGCOACCGAACAGCACAATC
Glyceraldehyde-3-phosphate dehydrogenase	*GAPDH*	GGAGCGAGATCCCTCCAAAAT	GGCTGTTGTCATACTTCTCATGG

RT-qPCR: Real-time quantitative polymerase chain reaction.

China) was followed the kit instructions for operation to detect apoptosis. Nuclei were counterstained with DAPI.

Reactive oxygen species detection Cells were incubated with the fluorescent probe 2',7'-dichlorodihydrofluorescein diacetate (DCFH-DA; 10 μmol/L; DCFH-DA Kit, Beyotime Biotechnology, China) for 20min, and the intracellular reactive oxygen species (ROS) levels were observed under a fluorescence microscope or quantitatively detected using a microplate reader.

Molecular Biology Detection

Western blot Total proteins from cells or retinal tissues were extracted using RIPA lysis buffer (Gibco Company, USA). After quantification by BCA assay, SDS-PAGE electrophoresis was performed and the proteins were transferred to polyvinylidene fluoride (PVDF) membranes (Millipore Corporation, USA). The membranes were blocked with 5% skim milk and then incubated with primary and secondary antibodies (Proteintech, USA) successively. The bands were visualized using an enhanced chemiluminescence (ECL) chemiluminescence system and analyzed for gray values with ImageJ software (ImageJ 1.53e software, National Institutes of Health, USA). Glyceraldehyde-3-phosphate dehydrogenase (GAPDH) was used as the internal reference. The target proteins detected included: NLRP3, apoptosis-associated speck-like protein containing a CARD (ASC), caspase-1, IL-1β, IL-18, vascular endothelial growth factor (VEGF), METTL3, and TXNIP (primary antibody, Abcam, USA).

RNA extraction and real-time quantitative PCR Total RNA was extracted using the TRIzol method and reverse transcribed to synthesize cDNA. Quantitative polymerase chain reaction (qPCR; PCR kit, TAKARA, Japan) was performed using the SYBR Green method, with GAPDH as the internal reference. The relative expression levels of genes were calculated by the $2^{-\Delta\Delta Ct}$ method. The primer (GenePharma, China) sequences are provided in Table 1.

Detection of m^{6}A methylation levels Total RNA was extracted from cells. Equal amounts of RNA (200-400 ng) were spotted onto positively charged nylon membranes and cross-linked by ultraviolet (UV). The membranes were probed with an anti-m^{6}A antibody, followed by incubation with horseradish peroxidase (HRP)-conjugated secondary antibody and developed. Methylene blue staining was used to verify the RNA loading.

Bioinformatics and Computational Simulation

Molecular docking The 3D structure of catalpol was obtained from PubChem (https://pubchem.ncbi.nlm.nih.gov/), and the protein structures of METTL3, NLRP3, TXNIP, and IL-1β were obtained from the AlphaFold database (https://alphafold.ebi.ac.uk/). AutoDockTools (AutodockTools 1.5.7, Molecular Graphics Laboratory, https://ccsb.scripps.edu/mgltools/) was used to process the proteins and ligands, and semi-flexible docking was performed using AutoDock Vina (AutoDock 4.2.6; http://vina.scripps.edu.), with the search space covering the known active pockets. The binding conformations were screened based on the binding free energy, and the interactions were visualized and analyzed using PyMOL (PyMol 3.1 Software; https://www.pymol.com/)[14-15].

Molecular dynamics simulation The simulation was conducted in GROMACS (version 2021.3, https://www.gromacs.org)[16-18]. The protein was modeled using the AMBER99SB-ildn force field, and the catalpol was modeled using the GAFF force field. The system was placed in a TIP3P water box and ions were added to neutralize the charge. After energy minimization, number of particles-volume-temperature (NVT) and number of particles-pressure-temperature (NPT) equilibration, a 100ns production simulation was carried out. The root mean square deviation, root mean square fluctuation, and binding free energy of the trajectory were analyzed to evaluate the stability of the complex.

Statistical Analysis Data were analyzed using GraphPad Prism 10.0 software (GraphPad Software Inc., San Diego, CA, USA). Each experiment was independently repeated at least three times to ensure reproducibility. Results are presented as mean±standard deviation (SD). Comparisons between two groups were performed using Student's *t*-test. For comparisons among three or more groups, one-way analysis of variance (ANOVA) was applied, followed by Tukey's post hoc test for multiple comparisons. A *P*-value of less than 0.05 was considered statistically significant.

RESULTS

Catalpol Improves Retinal Function and Vascular Integrity in Diabetic Mice After 14wk of intervention, compared with

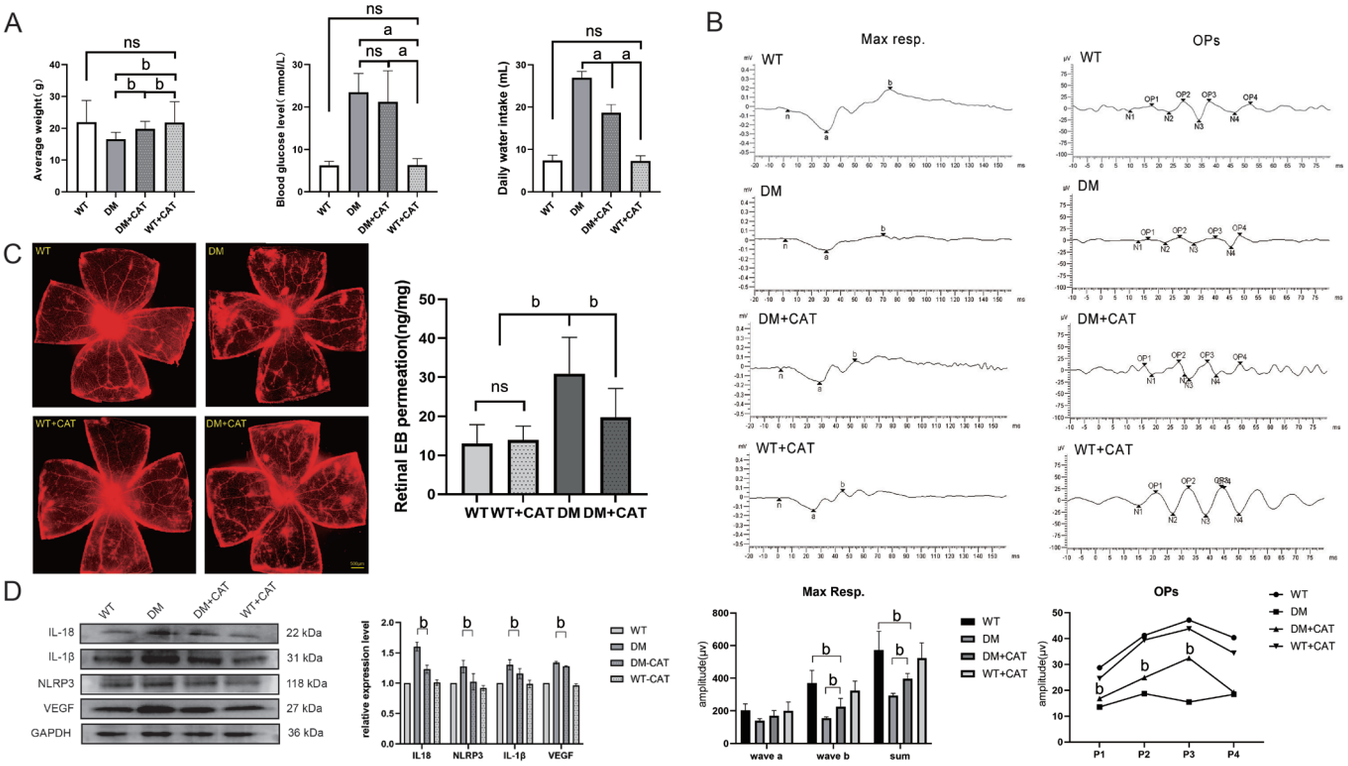

Figure 1 *In vivo* experiments, catalpol ameliorated retinal dysfunction and vascular leakage in diabetic mice, accompanied by suppression of NLRP3 inflammasome-related proteins A: General physiological indicators of the diabetic mouse model (after 14wk of intervention; n=6, ^aP<0.01; ^bP<0.05); B: The maximum response (Max Resp.) and the OPs; C: Evans blue staining fluorescence images. Quantitative statistics of retinal leakage; D: The relative protein expression levels of NLRP3, VEGF, IL-1β and IL-18 in the mouse retinal tissues (n=4, ^bP<0.05). ns: Not significant; WT: Wild type; DM: Diabetes mellitus; CAT: Catalpol; EB: Evans blue; IL: Interleukin; NLRP3: NOD-like receptor family pyrin domain containing 3; VEGF: Vascular endothelial growth factor; GAPDH: Glyceraldehyde-3-phosphate dehydrogenase; OPs: Oscillatory potentials.

WT group, the DM group mice exhibited typical "three more and one less" symptoms, including significant weight loss, increased water intake, and persistent hyperglycemia. Catalpol treatment (DM+CAT) partially alleviated the weight loss and polydipsia caused by diabetes, but had no significant effect on blood glucose levels (Figure 1A), suggesting that its protective effect does not depend on hypoglycemic action.

As shown in Figure 1B, compared with the WT group, the amplitudes of the a-wave, b-wave, and OPs of the dark-adapted maximum response in the DM group were significantly decreased, indicating that diabetes caused severe damage to the inner retinal neurons and vascular function. The treatment with catalpol effectively prevented the decline of these ERG amplitudes and significantly improved the retinal electrophysiological function of diabetic mice.

The EB leakage assay demonstrated a significant increase in retinal vascular leakage in the DM group of mice. However, treatment with catalpol significantly reduced the fluorescence intensity of EB, indicating that it can effectively alleviate the increased vascular permeability caused by diabetes and protect the integrity of the blood-retinal barrier (Figure 1C).

Western blot results showed that compared with the WT group, the protein expressions of NLRP3 inflammasome, VEGF, and mature forms of IL-1β and IL-18 in the retina of the DM group were significantly upregulated in retinal tissues. Catalpol treatment significantly reversed the abnormally high expression of these proteins (Figure 1D). These results suggest that the protective effect of catalpol *in vivo* is closely related to its inhibition of the NLRP3 inflammatory pathway and VEGF expression.

Catalpol Inhibits Inflammation, Oxidative Stress and Apoptosis Induced by High Glucose in HRVECs *In vitro* experiments, MTT and Calcein-AM/PI fluorescence double staining experiments indicated that catalpol at concentrations no higher than 0.5 mmol/L had no effect on the viability of HRVECs (Figure 2A, 2B) and could significantly reverse the decline in cell viability caused by HG (Figure 2C, 2D). Therefore, 0.5 mmol/L was selected as the working concentration of catalpol for subsequent experiments.

Then, Western Blot results showed that compared with the NG group, HG stimulation significantly upregulated the protein expression of NLRP3, the adaptor protein ASC, and the activated form of caspase-1 in HRVECs, and promoted the maturation and release of downstream inflammatory factors IL-1β and IL-18. Co-treatment with catalpol effectively inhibited the abnormal high expression of these proteins

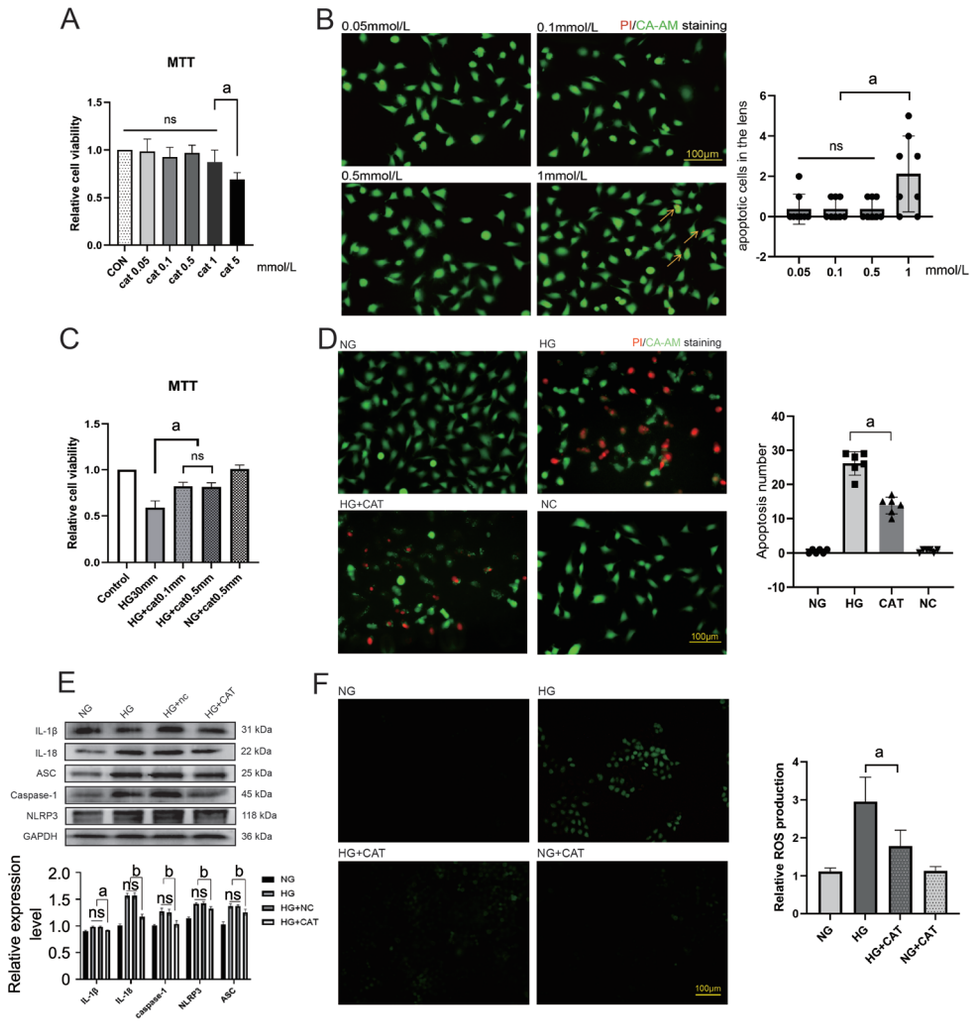

Figure 2 *In vitro* experiments, catalpol alleviated HG-induced NLRP3 inflammasome activation, oxidative stress, and apoptosis in HRVECs A: MTT assay shows cell viability of HRVECs pretreated with different concentrations of catalpol for 48h; B: PI/CA-AM staining show the apoptosis of HRVECs; C: The MTT assay was used to investigate the effect of different concentrations of catalpol on the cell viability of HRVECs after 48h of stimulation with HG (30 mmol/L); D: PI/CA-AM staining of HRVECs and analysis of cell apoptosis; E: The expression of IL-1β, IL-18, ASC, Caspase-1, and NLRP3 was detected by Western blotting; F: The DCFH-DA fluorescence method detect the level of ROS in HRVECs. n=4, ^aP<0.05, ^bP<0.01. ns: Not significant; HG: High glucose; NG: Normal glucose; NC: Normal control; CAT: Catalpol; IL: Interleukin; ASC: Apoptosis-associated speck-like protein containing a CARD; NLRP3: NOD-like receptor family pyrin domain containing 3; GAPDH: Glyceraldehyde-3-phosphate dehydrogenase; PI/CA-AM: Prodium Iodide/calcein acetoxymethyl; ROS: Reactive oxygen species; HRVECs: Human retinal vascular endothelial cells.

(Figure 2E), indicating that it could block HG-induced NLRP3 inflammasome activation.

Detection using the DCFH-DA fluorescent probe revealed that HG stimulation led to a sharp increase in ROS levels within HRVECs, while co-treatment with catalpol significantly alleviated this oxidative stress (Figure 2F). This result suggests that the anti-inflammatory effect of catalpol may be partially attributed to its antioxidant capacity.

Finally, the results of Calcein-AM/PI double staining both confirmed that HG stimulation significantly increased the apoptosis rate of HRVECs. After catalpol intervention, the number of apoptotic cells was significantly reduced and the cell survival rate was improved. In conclusion, catalpol can protect HRVECs from HG-induced cell damage and death by inhibiting oxidative stress and NLRP3 inflammasome activation.

Catalpol Exerts Protective Effects by Regulating METTL3-m^{6}A-TXNIP Axis Western blot results showed that HG stimulation significantly upregulated the protein expression of the core methyltransferase METTL3 in HRVECs. Consistent with this, dot blot experiments indicated that HG significantly increased the global m^{6}A methylation level of total cellular RNA. Co-treatment with catalpol effectively reversed the upregulation of METTL3 and the excessive m^{6}A modification (Figure 3A, 3B), suggesting that it may exert its effects by influencing the m^{6}A methylation system.

Bioinformatics analysis (SRAMP database) predicted that multiple potential m^{6}A modification sites exist on the

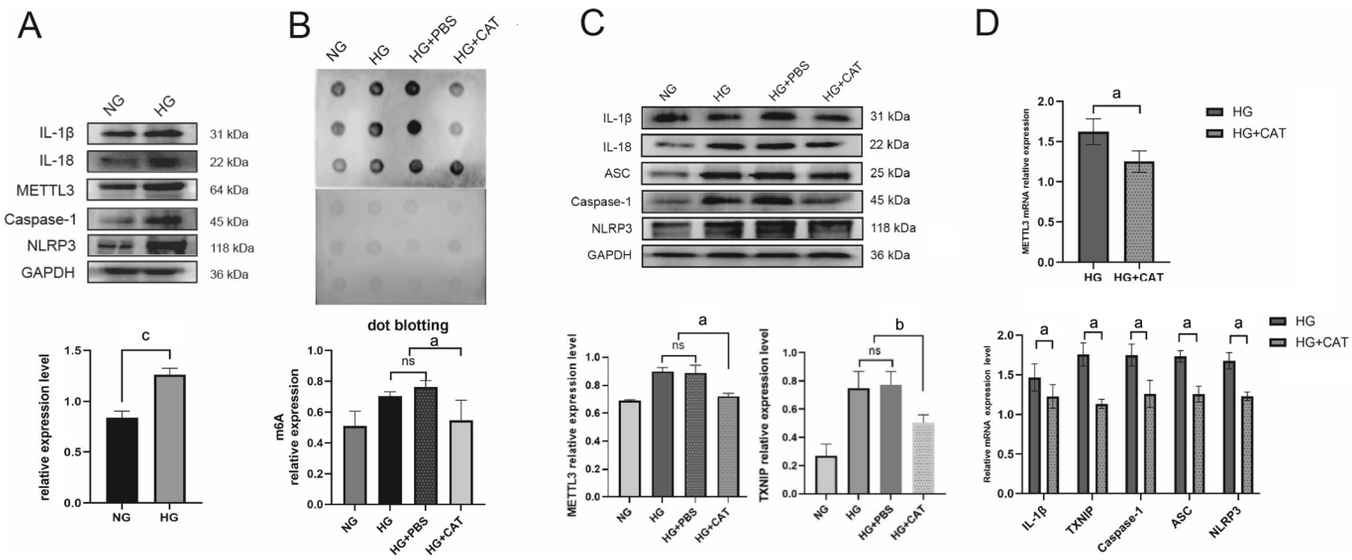

Figure 3 Catalpol inhibited the METTL3-m^{6}A-TXNIP axis and downstream NLRP3 inflammasome components under HG conditions A: Western blot detect METTL3 expression under HG conditions; B: Dot blot was used to detect and quantify m^{6}A methylation levels in total RNA; C: Western blot analysis of the expression changes of IL-1β, IL-18, TXNIP, METTL3, and NLRP3. Quantitative comparison of the relative expression changes of METTL3 and TXNIP; D: RT-PCR analysis of METTL3, TXNIP, and inflammatory complex expression under HG conditions. n=4, ^aP<0.05, ^bP<0.01, ^cP<0.0001. IL: Interleukin; METTL3: Methyltransferase-like 3; NLRP3: NOD-like receptor family pyrin domain containing 3; GAPDH: Glyceraldehyde-3-phosphate dehydrogenase; HG: High glucose; NG: Normal glucose; PBS: Phosphate buffer saline; CAT: Catalpol; ASC: Apoptosis-associated speck-like protein containing a CARD; ns: Not significant; TXNIP: Thioredoxin-interacting protein; RT-PCR: Real-time polymerase chain reaction; m^{6}A: N6-methyladenosine.

mRNA of TXNIP, a key molecule linking oxidative stress and inflammation. Experiments confirmed that HG not only induced METTL3 expression but also significantly upregulated the protein and mRNA levels of TXNIP. Catalpol could simultaneously inhibit the expression of METTL3 and TXNIP (Figure 3C, 3D). These changes were highly consistent with the activation state of the NLRP3 inflammasome, suggesting that METTL3-m^{6}A might affect downstream inflammation by regulating TXNIP.

To directly verify the core role of METTL3 in this pathway, we used the specific METTL3 inhibitor STM2457. The results showed that STM2457 could mimic the effect of catalpol. It significantly inhibited the global m^{6}A level increase induced by HG (Figure 4A), and simultaneously downregulated the expression of TXNIP and NLRP3 inflammasome-related proteins (NLRP3, ASC, Caspase-1, IL-1β; Figure 4B, 4C). Additionally, inhibition of METTL3 could also significantly alleviate the excessive ROS generation (Figure 4D) and apoptosis (Figure 4E) caused by HG.

These results collectively indicate that HG enhances m^{6}A modification by upregulating METTL3, which may stabilize pro-inflammatory transcripts such as TXNIP, ultimately driving NLRP3 inflammasome activation and endothelial injury. Catalpol exerts its downstream anti-inflammatory and antioxidant protective effects by targeting and inhibiting this METTL3-m^{6}A-TXNIP axis.

Molecular Docking and Dynamics Simulation Reveal the Stable Binding of Catalpol to Key Targets The molecular docking results showed that catalpol could stably bind to four key target proteins: NLRP3, IL-1β, TXNIP, and core methyltransferase METTL3, with binding free energies of -5.0, -6.0, -5.2, and -5.2 kcal/mol, respectively (Figure 5A). Among them, the binding affinities with IL-1β and METTL3 were the strongest, suggesting that catalpol may exert multi-target regulatory effects by directly acting on these proteins.

Catalpol mainly binds to target proteins through intermolecular forces such as hydrogen bonds (Figure 5B). For instance, it forms hydrogen bonds with key residues ASP395, SER511, and HIS512 in the catalytic pocket of METTL3; it also has strong hydrogen bond interactions with residues such as GLN14 and GLU110 in IL-1β. Hydrogen bond analysis showed that catalpol maintained a considerable and stable number of hydrogen bonds with METTL3, IL-1β, and TXNIP throughout the simulation (Figure 5C). These specific interactions provide a structural basis for the biological activity of catalpol.

The root mean square deviation and root mean square fluctuation of all complex systems reached equilibrium and remained at a low level in the later stage of the simulation (Figure 5D, 5E), indicating that the complex conformation was stable and the binding of catalpol to the protein had good dynamic stability. The free energy landscape analysis further indicated that each complex system was mainly concentrated in a low free energy basin, corresponding to a dominant

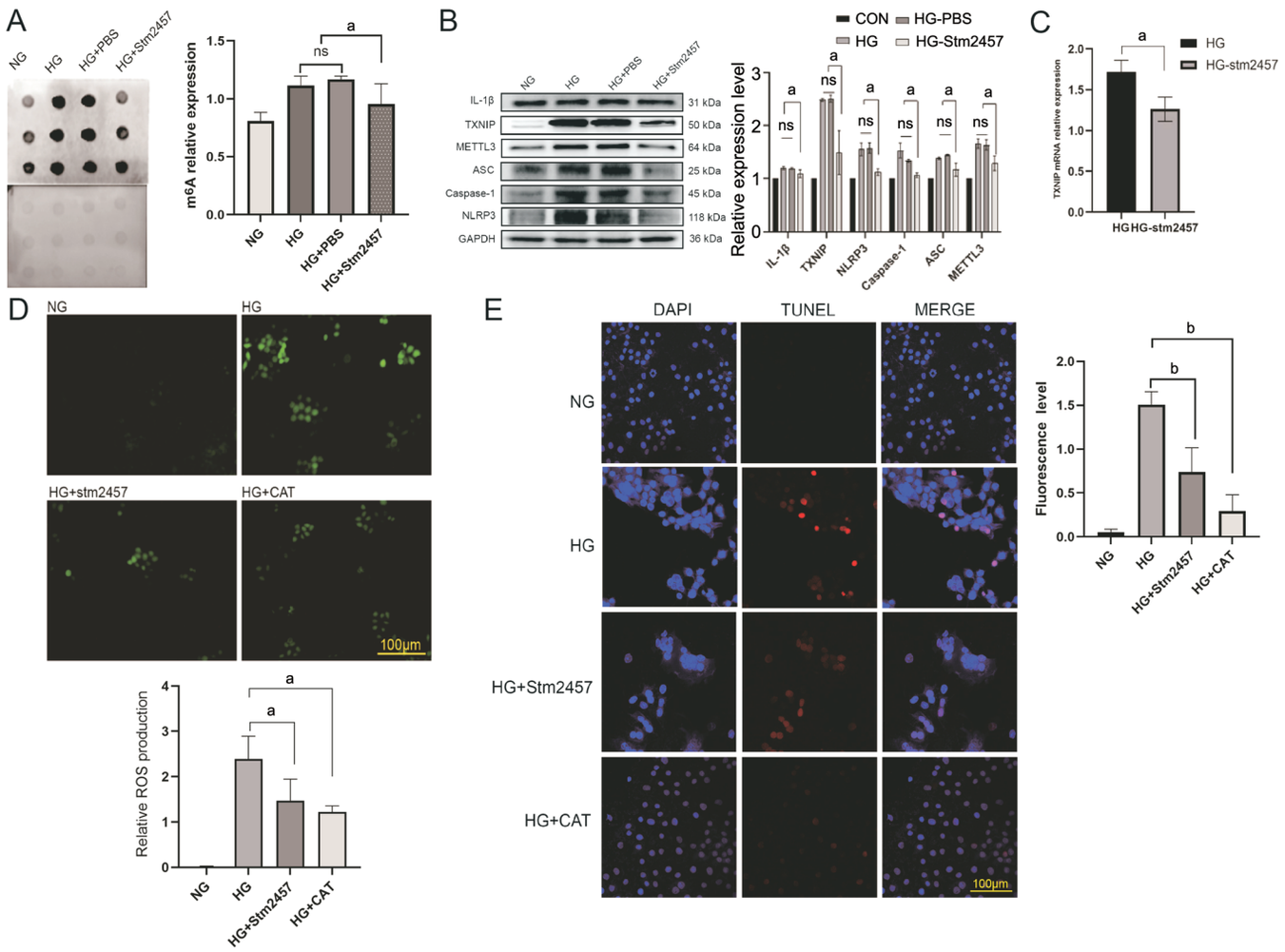

Figure 4 METTL3 inhibition by STM2457 recapitulated catalpol's effects, suppressing m^{6}A modification, TXNIP/NLRP3 pathway, oxidative stress, and apoptosis A: Dot blotting detection and quantitative comparison; B: Western blot detection of the expression of inflammasome; C: The expression level of TXNIP mRNA by RT-PCR; D: Fluorescence staining detect the ROS released by HRVECs in response to HG; E: DAPI/TUNEL fluorescence staining is used to detect the apoptosis status of HRVECs. *n*=4, ^aP<0.05, ^bP<0.001. ns: Not significant; GAPDH: Glyceraldehyde-3-phosphate dehydrogenase; HG: High glucose; NG: Normal glucose; PBS: Phosphate buffer saline; CAT: Catalpol; m^{6}A: N6-methyladenosin; IL: Interleukin; TXNIP: Thioredoxin-interacting protein; METTL3: Methyltransferase-like 3; ASC: Apoptosis-associated speck-like protein containing a CARD; NLRP3: NOD-like receptor family pyrin domain containing 3; CAT: Catalpol; ROS: Reactive oxygen species; DAPI: 4′,6-diamidino-2-phenylindole; TUNEL: Terminal-deoxynucleoitidyl transferase mediated nick end labeling; HRVECs: Human retinal vascular endothelial cells; RT-PCR: Real-time polymerase chain reaction.

conformational cluster (Figure 5F), which confirmed the binding stability from a thermodynamic perspective.

In summary, computational simulation studies have confirmed that catalpol can directly bind to key proteins (NLRP3, IL-1β, TXNIP) in the NLRP3 inflammatory pathway and the upstream regulatory factor METTL3 with high affinity and stability. This result provides theoretical computational support for the aforementioned experimental findings, especially offering important structural biological evidence for the regulatory role of catalpol through targeting METTL3.

DISCUSSION

This study for the first time systematically clarified the mechanism by which the active component of traditional Chinese medicine, catalpol, alleviates diabetic retinal vascular endothelial injury by targeting METTL3-m^{6}A methylation modification and inhibiting the TXNIP/NLRP3 inflammatory axis. This discovery not only provides new experimental evidence for the treatment of DR with catalpol, but also reveals the key role of epigenetic transcriptional regulation in diabetic microvascular complications.

This study confirmed the good safety of catalpol in diabetic animal models through long-term administration. Its protective effects on retinal function (ERG) and vascular barrier (EB leakage) are independent of hypoglycemic effects[19-20]. This is consistent with the multi-organ protective effects of catalpol in diabetic nephropathy, neuropathy and other complications reported in previous studies[8,20-23]. However, research on DR, a specific eye disease, is still blank. Our ERG data confirmed

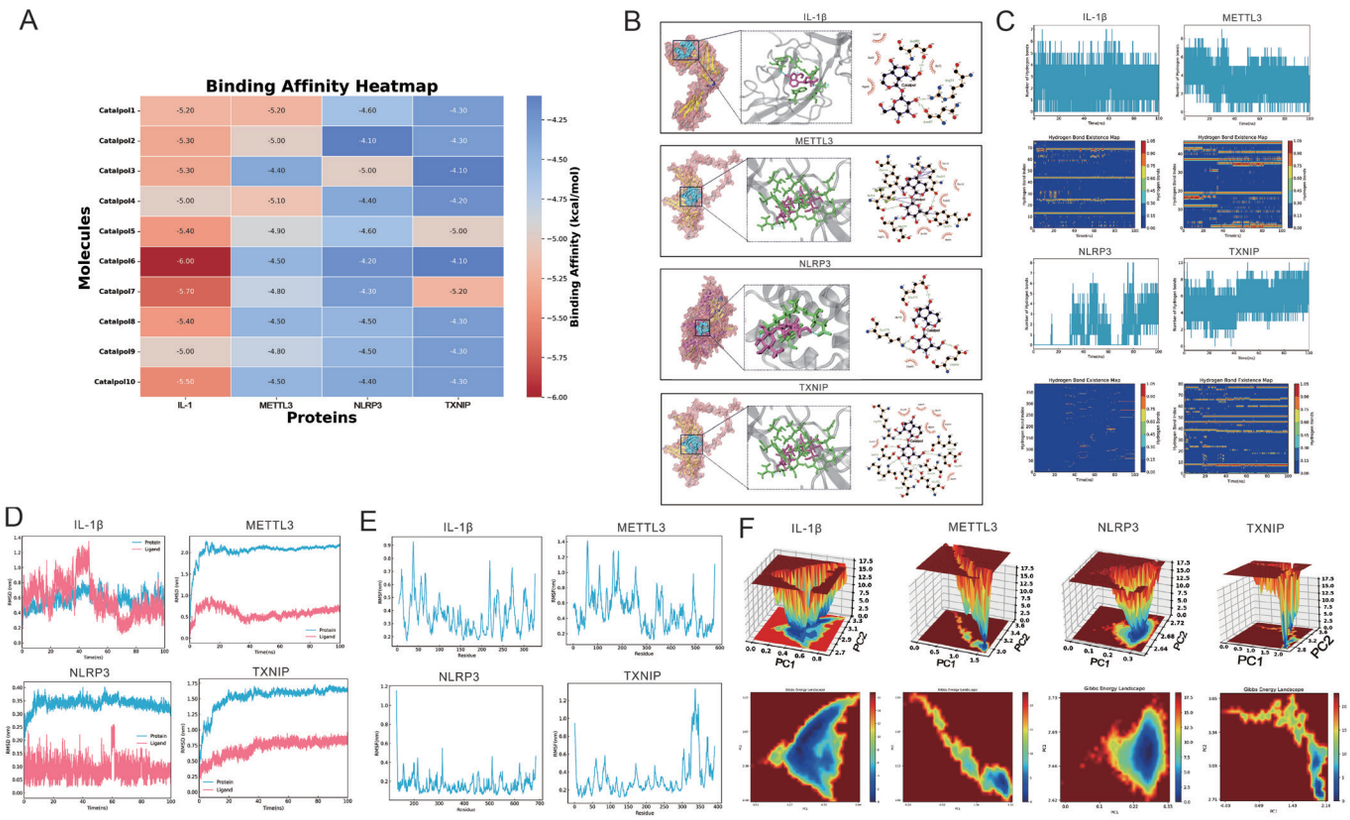

Figure 5 Molecular docking and molecular dynamics simulation A: The affinity heat map of Catalpol for IL-1β, METTL3, NLRP3, and TXNIP; B: The binding pocket models; C: The number and lifetime of hydrogen bonds; D: The root mean square deviation analysis of molecular dynamics simulation of the complex; E: The root mean square fluctuation analysis of molecular dynamics simulation of the complex; F: The free energy landscape profile of the complex. IL: Interleukin; METTL3: Methyltransferase-like 3; NLRP3: NOD-like receptor family pyrin domain containing 3; TXNIP: Thioredoxin-interacting protein.

that catalpol can significantly improve the damage to retinal neurons (OPs amplitude) and vascular function (b-wave) caused by diabetes[24-26], providing important functional evidence for its clinical transformation.

Chronic low-grade inflammation is a core pathological feature of DR[27-28]. This study confirmed that in the retinas of diabetic mice and HRVECs stimulated by HG, NLRP3 inflammasome and its downstream effector factors IL-1β/IL-18 were significantly activated[29-30]. This is consistent with the findings in the vitreous of PDR patients[31]. The activation of NLRP3 can disrupt the blood-retinal barrier by promoting IL-1β release and up-regulating the expression of adhesion molecules, *etc*.[32-34]. Our research shows that catalpol can effectively inhibit the expression of all key proteins (NLRP3, ASC, Caspase-1, IL-1β/IL-18) in this pathway and simultaneously reduce vascular leakage. This indicates that inhibiting the NLRP3 inflammasome is the key mechanism by which catalpol alleviates vascular inflammation in DR, which is consistent with the direction of action of other NLRP3 inhibitors in the literature (such as MCC950)[10].

Inhibition of the NLRP3 inflammasome has been established as a promising therapeutic approach for DR. This is supported by studies on various agents, such as the natural flavonoid quercetin[35] and the lipid-lowering drug fenofibrate[36], both of which have been shown to mitigate retinal endothelial injury by suppressing NLRP3 activation. While these findings validate the NLRP3 pathway as a crucial therapeutic node, the upstream regulatory mechanisms, particularly at the epitranscriptomic level, remain largely unexplored. Our study breaks new ground by demonstrating that catalpol, another natural compound, targets the novel METTL3-m^{6}A-TXNIP axis to inhibit NLRP3 inflammasome activation. m^{6}A modification is a recently highlighted epitranscriptional regulatory mechanism in metabolic diseases and their complications[9,37-39]. It is worth noting that METTL3-mediated m^{6}A modification has been proven to play a key role in the pathogenesis of other diabetic eye diseases, such as cataracts[40]. We confirmed that a HG environment upregulates the expression of the core writer enzyme METTL3 and the global m^{6}A level in HRVECs, and catalpol can reverse this phenomenon. Particularly importantly, we identified TXNIP as a key downstream target. TXNIP is a pivotal molecule connecting oxidative stress with NLRP3 inflammasome activation[11]. Through bioinformatics prediction and experimental verification, this study found that its expression is regulated by METTL3-mediated m^{6}A modification. The use of a specific METTL3 inhibitor,

STM2457, can perfectly simulate the effect of catalpol, simultaneously inhibiting m^{6}A modification, TXNIP/NLRP3 pathway upregulation, ROS generation, and cell apoptosis. This directly proves that METTL3-m^{6}A-TXNIP-NLRP3 is a core signaling axis through which catalpol exerts its effects. This discovery is consistent with the mechanism reported by Zhang *et al*[10] regarding METTL3 exacerbating inflammation in liver ischemia-reperfusion injury through m^{6}A modification of TXNIP, but it is the first time to be confirmed in a DR vascular endothelial model and associated with natural drug intervention.

The results of molecular docking and dynamics simulation provide structural-level support for the above findings. Catalpol can stably bind to four key targets, namely METTL3, NLRP3, TXNIP, and IL-1β, with the strongest affinity for METTL3 and IL-1β. This suggests that catalpol may, on the one hand, directly inhibit the enzymatic activity of METTL3 (affecting upstream modification), and on the other hand, directly antagonize the effect of IL-1β (blocking downstream inflammation), forming a multi-target and multi-level synergistic anti-inflammatory network. The study by She *et al*[41] also found that catalpol can inhibit microglial immune responses by interacting with NF-κB/NLRP3, further confirming its multi-target characteristics.

This study has several limitations. First, the STZ-induced type 1 diabetes model was used, and future validation is needed in type 2 diabetes models such as *db/db* mice. Second, although the focus was on METTL3, m^{6}A modification is a dynamic and reversible process involving “readers” and “erasers” (such as FTO and ALKBH5)[38,40], and it is worth exploring whether catalpol affects these proteins. We have not directly confirmed the function of specific m^{6}A sites on TXNIP mRNA through point mutation experiments. Additionally, the ocular pharmacokinetics of catalpol, the long-term safety of its use, and the optimal delivery system (such as nanofabrication) still require in-depth research. Future work should validate the correlation between METTL3/m^{6}A and the severity of DR in clinical samples and promote the translational research of catalpol as a novel, epitranscriptional-targeted treatment strategy for DR.

ACKNOWLEDGEMENTS

Authors’ Contributions: Conceptualization: Jiang Q, Yan F; Methodology: Liu JY, Zhu JY, Xiao YF; Investigation: Liu JY, Ge YR; Writing–Original Draft: Liu JY; Writing–Review & Editing: Jiang Q, Yan F; Supervision: Jiang Q, Yan F, Ge YR; Funding Acquisition: Liu JY, Ge YR, Yan F.

Foundations: Supported by the Hospital Management Research Projects of Jinling Hospital (No.2024JCYJQN113); Taikang Xianlin Gulou Hospital (No.TKKYZD20243501).

Conflicts of Interest: Liu JY, None; **Zhu JY,** None; **Xiao YF,** None; **Ge YR,** None; **Yan F,** None; **Jiang Q,** None.

REFERENCES

1 Zhou J, Chen B. Retinal cell damage in diabetic retinopathy. *Cells* 2023;12(9):1342.

2 Nian S, Lo ACY, Mi YJ, *et al*. Neurovascular unit in diabetic retinopathy: pathophysiological roles and potential therapeutical targets. *Eye Vis (Lond)* 2021;8(1):15.

3 Meng CR, Gu CF, He S, *et al*. Pyroptosis in the retinal neurovascular unit: new insights into diabetic retinopathy. *Front Immunol* 2021;12:763092.

4 Al Mamun A, Mimi AA, Zaeem M, *et al*. Role of pyroptosis in diabetic retinopathy and its therapeutic implications. *Eur J Pharmacol* 2021;904:174166.

5 O’Leary F, Campbell M. The blood–retina barrier in health and disease. *FEBS J* 2023;290(4):878-891.

6 Wang YJ, Liao DQ, Qin MJ, *et al*. Simultaneous determination of catalpol, aucubin, and geniposidic acid in different developmental stages of *Rehmannia glutinosa* leaves by high performance liquid chromatography. *J Anal Meth Chem* 2016;2016:4956589.

7 Bai Y, Zhu RY, Tian YM, *et al*. Catalpol in diabetes and its complications: a review of pharmacology, pharmacokinetics, and safety. *Molecules* 2019;24(18):3302.

8 Chen J, Yang YW, Lv ZY, *et al*. Study on the inhibitive effect of Catalpol on diabetic nephropathy. *Life Sci* 2020;257:118120.

9 Hsu PJ, Zhu YF, Ma HH, *et al*. Ythdc2 is an N^6-methyladenosine binding protein that regulates mammalian spermatogenesis. *Cell Res* 2017;27(9):1115-1127.

10 Zhang Y, Lv JR, Bai J, *et al*. METTL3 modulates TXNIP expression to affect the activation of NLRP3 inflammasome in hepatic cells under oxygen–glucose deprivation/reperfusion injury. *Inflammation* 2024;47(3):1028-1040.

11 He SK, Yaung J, Kim YH, *et al*. Endoplasmic reticulum stress induced by oxidative stress in retinal pigment epithelial cells. *Graefes Arch Clin Exp Ophthalmol* 2008;246(5):677-683.

12 Li ZJ, Meng XY, Chen Y, *et al*. N^6-methyladenosine (m^{6}A) writer METTL3 accelerates the apoptosis of vascular endothelial cells in high glucose. *Heliyon* 2023;9(3):e13721.

13 Shi KP, Li YT, Huang CX, *et al*. Evans blue staining to detect deep blood vessels in peripheral retina for observing retinal pathology in early-stage diabetic rats. *Int J Ophthalmol* 2021;14(10):1501-1507.

14 Eberhardt J, Santos-Martins D, Tillack AF, *et al*. AutoDock vina 1.2.0: new docking methods, expanded force field, and Python bindings. *J Chem Inf Model* 2021;61(8):3891-3898.

15 Trott O, Olson AJ. AutoDock Vina: improving the speed and accuracy of docking with a new scoring function, efficient optimization, and multithreading. *J Comput Chem* 2010;31(2):455-461.

16 Abraham MJ, Murtola T, Schulz R, *et al*. GROMACS: high performance molecular simulations through multi-level parallelism from laptops to supercomputers. *SoftwareX* 2015;1-2:19-25.

17 Case DA, Aktulga HM, Belfon K, *et al*. AmberTools. *J Chem Inf Model* 2023;63(20):6183-6191.

18 Kumari R, Kumar R, *et al*. *g_mmpbsa*—a GROMACS tool for high-throughput MM-PBSA calculations. *J Chem Inf Model* 2014;54(7):1951-1962.

19 Jiang TZ, Zhao R, Jiang B. Protective effect of catalpol in mice injuries induced by rotenone and evaluation of the safety of catalpol. *Prog Mod Biomed* 2008;8:1039-1041.

20 Fei BG, Dai W, Zhao SH. Efficacy, safety, and cost of therapy of the traditional Chinese medicine, catalpol, in patients following surgical resection for locally advanced colon cancer. *Med Sci Monit* 2018;24:3184-3192.

21 Zhu HF, Wang Y, Liu ZQ, *et al*. Antidiabetic and antioxidant effects of catalpol extracted from *Rehmannia glutinosa* (Di Huang) on rat diabetes induced by streptozotocin and high-fat, high-sugar feed. *Chin Med* 2016;11(1):25.

22 Shieh JP, Cheng KC, Chung HH, *et al*. Plasma glucose lowering mechanisms of catalpol, an active principle from roots of *Rehmannia glutinosa*, in streptozotocin-induced diabetic rats. *J Agric Food Chem* 2011;59(8):3747-3753.

23 Zhang ZX, Dai YG, Xiao YC, *et al*. Protective effects of catalpol on cardio-cerebrovascular diseases: a comprehensive review. *J Pharm Anal* 2023;13(10):1089-1101.

24 Tzekov R, Arden GB. The electroretinogram in diabetic retinopathy. *Surv Ophthalmol* 1999;44(1):53-60.

25 Pescosolido N, Barbato A, Stefanucci A, *et al*. Role of electrophysiology in the early diagnosis and follow-up of diabetic retinopathy. *J Diabetes Res* 2015;2015:319692.

26 Cobb WA, Morton HB. A new component of the human electroretinogram. *J Physiol* 1954;123:36P–37P.

27 Li XD, Zhou H. Targeting retinal neuroglial vascular unit damage: novel therapeutic strategies for early-stage diabetic retinopathy. *J Diabetes Res* 2025;2025:6922946.

28 Xu GT, Zhang JF, Tang L. Inflammation in diabetic retinopathy: possible roles in pathogenesis and potential implications for therapy. *Neural Regen Res* 2023;18(5):976-982.

29 Schroder K, Tschopp J. The inflammasomes. *Cell* 2010;140(6):821-832.

30 Shi HQ, Zhang Z, Wang XD, *et al*. Inhibition of autophagy induces IL-1β release from ARPE-19 cells *via* ROS mediated NLRP3 inflammasome activation under high glucose stress. *Biochem Biophys Res Commun* 2015;463(4):1071-1076.

31 Shen JK, Choy DF, Yoshida T, *et al*. Interleukin-18 has antipermeablity and antiangiogenic activities in the eye: reciprocal suppression with VEGF. *J Cell Physiol* 2014;229(8):974-983.

32 Grebe A, Hoss F, Latz E. NLRP3 inflammasome and the IL-1 pathway in atherosclerosis. *Circ Res* 2018;122(12):1722-1740.

33 Rheinheimer J, de Souza BM, Cardoso NS, *et al*. Current role of the NLRP3 inflammasome on obesity and insulin resistance: a systematic review. *Metabolism* 2017;74:1-9.

34 Yang Y, Wang HN, Kouadir M, *et al*. Recent advances in the mechanisms of NLRP3 inflammasome activation and its inhibitors. *Cell Death Dis* 2019;10(2):128.

35 Li R, Yao GM, Yan HL, *et al*. Effects of quercetin on diabetic retinopathy and its association with NLRP3 inflammasome and autophagy. *Int J Ophthalmol* 2021;14(1):42-49.

36 Shi Y, Liu AH, Li XR. Fenofibrate mitigates the dysfunction of high glucose-driven human retinal microvascular endothelial cells by suppressing NLRP3 inflammasome. *Int J Ophthalmol* 2025;18(5):792-801.

37 Benak D, Benakova S, Plecita-Hlavata L, *et al*. The role of m^6A and m^6Am RNA modifications in the pathogenesis of diabetes mellitus. *Front Endocrinol (Lausanne)* 2023;14:1223583.

38 An YY, Duan H. The role of m6A RNA methylation in cancer metabolism. *Mol Cancer* 2022;21(1):14.

39 Kumari R, Ranjan P, Suleiman ZG, *et al*. mRNA modifications in cardiovascular biology and disease: with a focus on m6A modification. *Cardiovasc Res* 2022;118(7):1680-1692.

40 Yang J, Liu JS, Zhao SZ, *et al*. N^6-methyladenosine METTL3 modulates the proliferation and apoptosis of lens epithelial cells in diabetic cataract. *Mol Ther Nucleic Acids* 2020;20:111-116.

41 She Y, Shao CY, Liu YF, *et al*. Catalpol reduced LPS induced BV2 immunoreactivity through NF-κB/NLRP3 pathways: an in vitro and in silico study. *Front Pharmacol* 2024;15:1415445.